

Hydrodynamic simulations of moonlet induced propellers in Saturn's rings: Application to Blériot

Martin Seiß(1), Nicole Albers(2), Miodrag Sremčević(2),
Jürgen Schmidt(3,1), Heikki Salo(3), Michael Seiler(1), Holger Hoffmann(1),
Frank Spahn(1)

(1) Theoretical Physics, Planetology group, Department of Physics and Astronomy,
University of Potsdam, Germany

(2) LASP, University of Colorado, Boulder, USA

(3) Astronomy Research Unit, University of Oulu, Finland

email: martin.seiss@uni-potsdam.de

January 18, 2017

Abstract

Small moons (moonlets) embedded in Saturn's rings cause S-shaped density structures in their close vicinity called propellers. These structures have been predicted by Spahn and Sremčević (2000) and Sremčević et al. (2002). N-body simulations later not only confirmed the formation of a propeller but additionally showed the appearance of wakes induced by the moonlet in the region adjacent to the S-shaped gaps (Seiß et al., 2005; Sremčević et al., 2007; Lewis and Stewart, 2009). One of the biggest successes of the Cassini mission is the detection of propeller structures in images taken by the Imaging Science Subsystem (ISS) of the spacecraft (Tiscareno et al., 2006).

Here, we present isothermal hydrodynamic simulations of moonlet induced propellers in Saturn's A ring. These allow for a combined treatment of gravitational scattering and diffusion and denote a further development of the original model (Spahn and Sremčević,

2000; Sremčević et al., 2002) where gravitational scattering of particles by the moonlet (creating the structure) and diffusion described by the hydrodynamic equations (smearing out the structure) had to be treated separately. We find excellent agreement between these new hydrodynamic and corresponding N-body simulations. Furthermore, the hydrodynamic simulations confirmed the scaling laws predicted by Spahn and Sremčević (2000) and an analytical solution derived by Sremčević et al. (2002). Finally, we match results from hydrodynamic simulations of the giant propeller Blériot to two stellar occultation observations by the Cassini Ultraviolet Imaging Spectrometer (UVIS). Best fits of the optical depth profiles are achieved using a Hill radius of 600 m and a kinematic shear viscosity of the surrounding ring material of $350 \text{ cm}^2/\text{s}$. The results imply a moonlet diameter of about 900 m.

1 Introduction

Saturn's dense rings consist of icy particles with sizes of centimeters up to tens of meters. Apart from this main population, small moons are embedded in these rings, which cause structures in the ring density by their gravitational influence. The largest examples are the two ring-moons Pan and Daphnis with radii of about 14 and 4 km, respectively (Showalter, 1991; Porco, 2005), massive enough to open and maintain a circumferential gap around their orbit (Henon, 1981; Lissauer et al., 1981; Petit and Henon, 1988; Spahn and Wiebicke, 1989; Spahn and Sponholz, 1989). Additional features caused by these moons are the central ringlet (Dermott et al., 1980; Dermott and Murray, 1981; Spahn and Sponholz, 1989) in case of Pan as well as wavy gap edges and the corresponding wakes (Cuzzi and Scargle, 1985; Showalter et al., 1986; Borderies et al., 1989; Spahn et al., 1994; Hertzsch et al., 1997; Lewis and Stewart, 2000; Weiss et al., 2009; Seiß et al., 2010).

Smaller moons (moonlets) with radii between 50 m and 500 m cannot be observed directly, but they reveal themselves by much larger S-shaped density structures in their vicinity, called propeller, caused by their gravitational interaction with the surrounding ring material (Spahn and Sremčević, 2000; Sremčević et al., 2002). More than 150 propeller structures have been detected in the A ring (Tiscareno et al., 2006; Sremčević et al., 2007; Tiscareno et al., 2008). The propeller named Blériot is the largest example, large enough to be tracked over a larger time span in the Cassini images. Analysis of the moonlets's orbital evolution revealed an unexplained wandering of its

longitude with respect to the motion from the expected Keplerian angular speed induced by the gravity of the planet (Tiscareno et al., 2010).

First investigations describing the density structure in the vicinity of a small embedded moonlet in the rings have been made by Spahn and Sremčević (2000). They used a model that combines gravitational scattering in the vicinity of the moon opening two gaps in the rings and diffusion leading to a closure of the gaps. This model predicted a structure consisting of two radially shifted gaps with limited azimuthal extent. Furthermore, they derived scaling laws that relate (a) the radial dimension of the gaps to the Hill radius of the moon

$$h = a \left(\frac{M_m}{3 M_p} \right)^{1/3} \quad (1)$$

and (b) the azimuthal extent of the gaps to the shear viscosity ν_0 of the ring flow and the mass of the moon $M_m/\nu_0 \propto h^3/\nu_0$. The semi-major axis and mass of the moon is denoted by a , whereas the mass of the planet is labeled by M_p . Sremčević et al. (2002) presented an analytical solution for the gap density. An extension of the model to the vertical degree of freedom was developed by Hoffmann et al. (2013, 2015), which explained the shape of the shadow cast by the propeller Earhart on the rings in Cassini images taken close to Saturn’s vernal equinox in August 2009.

For the first time, N-body simulations were used by Seiß et al. (2005) to investigate the moonlet induced propeller structure, which led to an inclusion of the wakes and to a confirmation of the predicted scaling laws. After the first propellers were detected, further N-body simulations were published including self-gravity (Sremčević et al., 2007; Lewis and Stewart, 2005), a ring particle size distribution (Lewis and Stewart, 2005) and also freely moving moonlets, not fixed to the center of the co-moving simulation box (Lewis and Stewart, 2005; Rein and Papaloizou, 2010).

N-body simulations are a powerful tool to investigate the formation of propellers, but they are computationally expensive, so that usually only the closer vicinity of a small moonlet can be simulated. The problem is that the size of the simulated ring particles has to be about 1 meter to get the right macroscopic properties of the ring as for example velocity dispersion, viscosity and pressure. Thus, with growing simulation area the number of simulated particles becomes prohibitively large. In order to lift this limitation, we use the hydrodynamic approach with values for pressure and transport coefficients determined from N-body simulations (Salo et al., 2001;

Daisaka et al., 2001) or directly from observations (Tiscareno et al., 2007; Sremčević et al., 2008). Hydrodynamic simulations are used here to simulate propellers for the first time, whereas this numerical method is an established tool to investigate the evolution of planetary embryos in a pre-planetary disk (e.g. Kley, 1999; Lubow et al., 1999), a system physically similar to moonlets embedded in a planetary ring.

In the following, the hydrodynamic equations are introduced in Section 2 and the simulation method is sketched in the Section 3. Results are presented and discussed in the Sections 4 and 5.

2 Hydrodynamic equations

Physically, the ring particles form a dense granular gas orbiting in a disk around the planet perturbed by a small moonlet embedded in the disk. The evolution of the surface mass density Σ and the flux $\Sigma \mathbf{v}$ of the ring material in a co-rotating frame are described by the continuity equation

$$\partial_t \Sigma + \nabla \cdot \Sigma \mathbf{v} = 0 \quad (2)$$

and the Navier-Stokes equations

$$\partial_t \Sigma \mathbf{v} + \nabla \cdot (\Sigma \mathbf{v} \circ \mathbf{v}) = -\Sigma \nabla \cdot (\Phi_p + \Phi_m) + \mathbf{f}_i - \nabla \cdot \hat{\mathbf{P}} \quad (3)$$

written here in the flux conserved form. The symbol \circ denotes the tensor product and the gravitational potentials of central planet and moonlet are labeled by Φ_p and Φ_m , respectively. The inertial forces in the co-rotating frame are the centrifugal and Coriolis force

$$\mathbf{f}_i = \Sigma \boldsymbol{\Omega} \times (\boldsymbol{\Omega} \times \mathbf{r}) + 2\Sigma \boldsymbol{\Omega} \times \mathbf{v} \quad (4)$$

respectively, where $\boldsymbol{\Omega}$ denotes the Kepler frequency of the moonlet. Note, we neglect here higher gravitational moments of Saturn treating it as a spherical planet.

The pressure tensor $\hat{\mathbf{P}}$ can be described with the Newtonian ansatz as

$$P_{ij} = p \delta_{ij} - \Sigma \nu \left(\frac{\partial v_i}{\partial x_j} + \frac{\partial v_j}{\partial x_i} \right) + \Sigma \left(\frac{2}{3} \nu - \xi \right) \nabla \cdot \mathbf{v} \delta_{ij} \quad (5)$$

where p , ν and ξ denote the scalar pressure as well as the kinematic shear and bulk viscosities, respectively. The pressure and the viscosities depend

on the local density, where we use power law relations describe this effect

$$p = p_0 \left(\frac{\Sigma}{\Sigma_0} \right)^\alpha \quad (6)$$

$$\nu = \nu_0 \left(\frac{\Sigma}{\Sigma_0} \right)^\beta. \quad (7)$$

Furthermore, the ratio between shear and bulk viscosity is set constant

$$\xi = \frac{\xi_0}{\nu_0} \cdot \nu. \quad (8)$$

In the simplest case, the unperturbed pressure is given by the ideal gas relation $p_0 = \Sigma_0 c_0^2$ at equilibrium, where c_0 denotes the dispersion velocity. We use an isothermal model, thus, the dispersion velocity c_0 and the related granular temperature $T = c_0^2/3$ are constant.

3 Method

Propellers are small objects in comparison to the ring dimensions and thus just a small region of the ring is simulated where the reference frame is fixed at the position of the moonlet on a circular orbit. The acting forces can be linearized and describe the Hill problem (Hill, 1878). In the following, x labels the radial distance from the moonlet in outward direction and y denotes the azimuthal orbit direction. The simulation program calculates the perturbed flux $\Sigma \mathbf{u}$ using the velocity $\mathbf{u} = \mathbf{v} + 3/2\Omega x \mathbf{e}_y$, which is reduced by the Keplerian shear velocity. The systematic shear velocity $-3/2\Omega x$ arises from the linearized radial dependence of the Kepler velocity. The Kepler frequency is calculated by $\Omega = \sqrt{GM_p/a^3}$ at the radial location of the moonlet a and the gravitational constant is labeled by G . Introducing $\Sigma \mathbf{u}$ simplifies the equations and increases the stability of the advection scheme introduced later. Thus, the Navier-Stokes equation reads now

$$\partial_t \Sigma \mathbf{u} + \nabla \cdot (\Sigma \mathbf{u} \circ \mathbf{v}) = -\Sigma \nabla \cdot \Phi_m + \mathbf{f}_T - \nabla \cdot \hat{\mathbf{P}} \quad (9)$$

The remaining inertial forces in this system can be written in the form

$$\mathbf{f}_T = 2\Omega \Sigma u_y \mathbf{e}_x - \frac{1}{2}\Omega \Sigma u_x \mathbf{e}_y. \quad (10)$$

The gravitational potential of the moon

$$\Phi_m = -\frac{GM_m}{\sqrt{x^2 + y^2 + \epsilon^2}} \quad (11)$$

is modified by a smoothing radius ϵ limiting the gravitational potential in the close vicinity of the moon center, usually a value $\epsilon = 0.2h$ is chosen.

The calculation region is a rectangular cutout of the ring with dimensions (x_{\min}, x_{\max}) and (y_{\min}, y_{\max}) with the moon in the center and it is divided into $N_x \times N_y$ equal-sized cells. The complete set of equations is integrated until a steady state is established. For the numerical integration the Navier-Stokes equation is split in x and y directions. This has the big advantage that the code can be easily parallelized. The advection term is solved with the first order donor-cell algorithm, which is easy to implement, but unfortunately induces an artificial diffusion. For this reason, we make sure that the resolution is sufficiently high and the results are not affected. For the simulations of Blériot, we use a second order scheme with MinMod flux limiter (LeVeque, 2002) in order to better conserve the wake crests. The influence of pressure and viscous transport is solved with an explicit scheme.

The advective time step is chosen as

$$\Delta t_{\text{ad}} = \frac{1}{2} \min \left(\frac{\Delta x}{(|v_x| + c)}, \frac{\Delta y}{(|v_y| + c)} \right) \quad (12)$$

to fulfill the Courant-Friedrichs-Lewy condition, necessary for a stable algorithm. The viscous time step is calculated from

$$\Delta t_{\text{vis}} = \min \left(\frac{\Delta x^2}{\nu}, \frac{\Delta y^2}{\nu} \right). \quad (13)$$

Usually the advective time step is much smaller than the viscous time step, and thus, sets the computation time step in our simulations.

At the borders of the calculation regions the boundary conditions are chosen such that the perturbations can flow out of the box freely, but the inflow is unperturbed. This is especially important at the azimuthal boundaries, where due to Kepler shear the material is flowing into the box at $x < 0, y = y_{\min}$ and $x > 0, y = y_{\max}$ and flowing out at $x < 0, y = y_{\max}$ and $x > 0, y = y_{\min}$. The influence of the moonlet is established mainly by its gravity. We also tested the influence of reflective boundary conditions on

its surface at radius R_m , but could not find a significant influence on the propeller pattern.

In the simulation time is scaled by $1/\Omega$ and length by h . Because the self-gravity of the ring material is neglected the background surface mass density is not important and is usually set to 1.

4 Results

The surface mass density distribution resulting from our hydrodynamic propeller simulation is plotted in the left panel of Figure 1. In this Figure, the simulation region is divided into $N_x \times N_y = 1200 \times 4000$ cells and spans from $-15h$ to $15h$ in radial and $-200h$ to $+200h$ in azimuthal direction. A steady state establishes after about 20 orbits. The parameters for the hydrodynamic simulations are set to $c_0 = 0.14 h\Omega$, $\alpha = 2.15$, $\nu_0 = 0.006 h^2\Omega$, $\xi_0 = 0.017 h^2\Omega$ and $\beta = 0.67$ (compare to: Salo et al., 2001).

The density pattern shows the typical propeller fingerprint with two radially displaced gaps showing density minima at about $x = \pm 2h$ which smooth out downstream. Particles, which pass the moon in larger radial distance, are deflected just slightly towards the moon. This induces a coherent motion of the ring material and in consequence the formation of wakes (Showalter et al., 1986).

4.1 Comparison with N-body simulations

Here, we compare the density structure from the hydrodynamic simulation with those obtained from N-body simulations using a local code developed in Salo (1995). This code was applied to propeller in Seiß et al. (2005) giving the opportunity to validate our hydrodynamic approach. This is not only important in order to judge the performance of our numerical schemes used. It also provides an opportunity to check the hydrodynamic approximation for this problem, including the isothermal model used here and the parameterisation of the viscosities and the pressure. The hydrodynamic approach requires that the mean free path and the size of the particles are much smaller than the length of the macroscopic structure investigated and than the epicyclic length caused by the thermal motion of the particles. Henceforth, the collision frequency and the inverse collision duration of the particles should be shorter than one orbital period. These assumptions are not always fulfilled

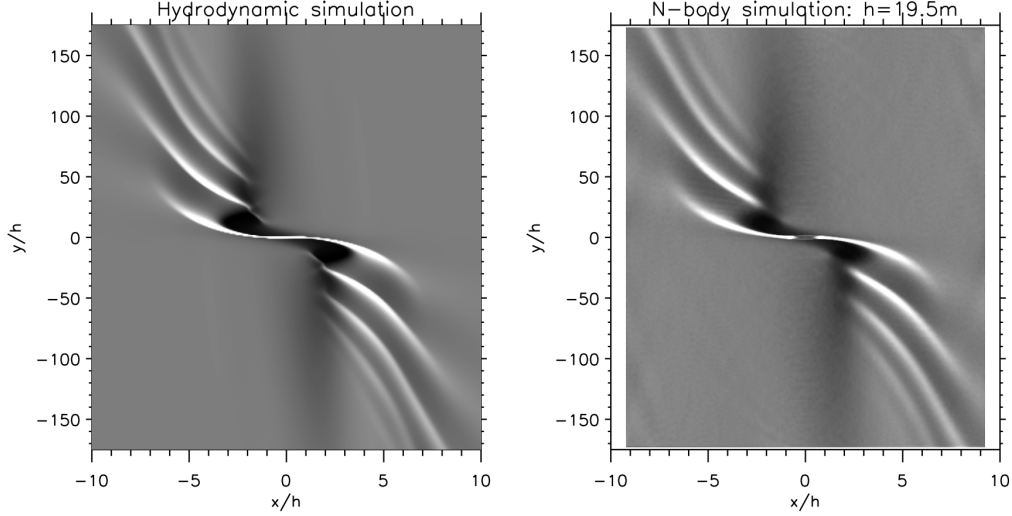


Figure 1: Propeller structure around a moonlet located in the center of the box. The axes are scaled by the Hill radius where x and y denote the radial direction outwards from the central planet and the azimuthal direction, respectively. The left panel presents the surface density from a hydrodynamic simulation whereas the right panel shows the resulting surface density from N-body simulation composed from 50 averaged snapshots taken every 0.1 orbits. The parameters for the hydrodynamic simulation are gained directly from the N-body simulations: $c_0 = 0.14 h\Omega$, $\alpha = 2.15$, $\nu_0 = 0.006 h^2\Omega$, $\xi_0 = 0.017 h^2\Omega$ and $\beta = 0.67$.

in the rings, especially in the regions of very low and high densities (see e.g. discussion in Seiß and Spahn, 2011).

The propeller are observed in the A ring and there the particles are meter sized and the mean free path is of the same order, leading to about 10 collisions per orbit per particle. On the one hand, the gaps are a few Hill radii wide in radial direction and their closure would take many orbits. Thus, hydrodynamics should work well here. On the other hand, the wakes are winding up along the azimuthal direction getting tighter and tighter wound, and furthermore, the particles need just one orbit to pass a single wake crest, so that a local thermodynamic equilibrium may not always establish.

For comparison a N-body simulation was performed with $N = 480,000$ particles with radii $R = 1$ m in a box size of $L_x \times L_y = 180 \text{ m} \times 3375 \text{ m}$ with a moon in the center having a radius of $R_m = 15$ m. Together with the bulk density of ice $\rho = 410 \text{ kg/m}^3$ the Hill radius of the moonlet becomes

$h = 19.5 \text{ m}$ ($a = 130,000 \text{ km}$). The geometric optical depth in the box, defined by

$$\tau = \frac{\pi R^2 N}{L_x L_y} , \quad (14)$$

is chosen as $\tau = 0.6$ - a value representative for the A ring.

The density pattern from the N-body simulation is presented in the right panel of Figure 1 and for comparison the left panel shows the hydrodynamic result, where pressure and transport parameters are gained from the N-body simulation. At a first glimpse both results look nearly identical. A more detailed comparison of the profiles in Figure 2 reveals an excellent agreement for the gap closing (upper left panel). Apart from boundary effects the profiles of the wakes agree also well (upper right panel) as long as the wake crests do not become too tight. Furthermore, the finite size of the ring particles smooth out the wake crests in the N-body simulation. However, this effect should play a smaller role for the large propeller Blériot modeled later. Summarizing, the N-body and hydrodynamic simulations of the propeller show a very good agreement. This encourages us to apply the hydrodynamic code to the large A-ring propellers orbiting between the Encke and Keeler gap which are too large to be modeled by N-body simulations. Note, the self-gravity of the disk is omitted in our test but the self-gravity wakes are much smaller in size than the pattern of the Trans-Encke propeller.

4.2 Radial and azimuthal scaling of the propeller gap

The radial structure of the gap in the close vicinity of the moon is mainly caused by the gravitational scattering by the moonlet. The equations of motion can be scaled by the Hill radius h if one neglects viscous transport and pressure. Thus, the Hill radius is the final radial scale of the density structure. This is demonstrated in Figure 3 (left panel), where the azimuthally averaged radial profiles (y/h from 0 to 100) are plotted using different values of the viscosity. The gap minimum and the adjacent maximum are located in all simulations at about $-2h$ and $-4h$ for $y > 0$, respectively. Different values for the viscosities change mainly only the density level, but not the location of minima and maxima. Insofar, the radial location of the gap minimum carries information about the mass of the moonlet.

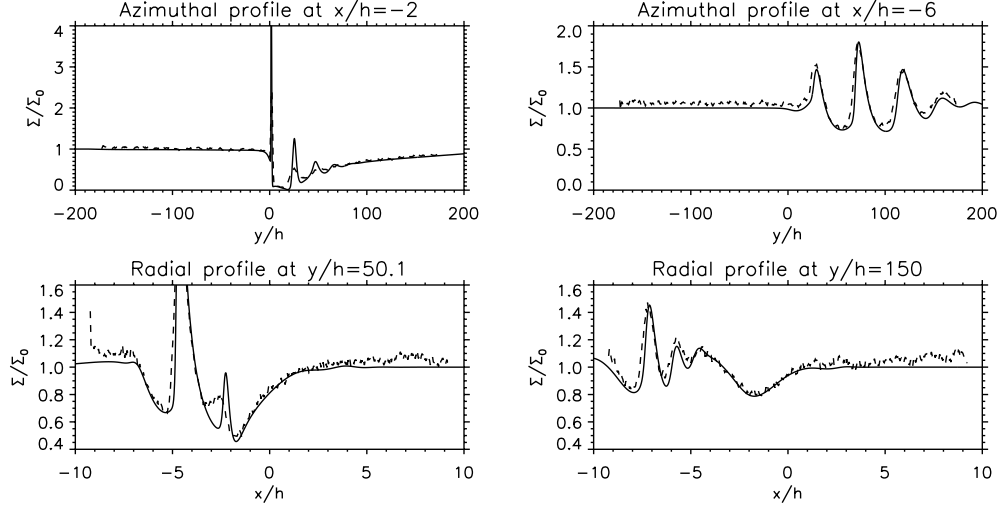


Figure 2: Comparison between hydrodynamic (solid lines) and N-body (dashed lines) simulations of a propeller. The profiles represent cuts along the azimuthal (upper panel) and the radial (lower panels) direction at various locations.

Sremčević et al. (2002) showed that the azimuthal structure should scale with the diffusion length as

$$aK = \frac{\Omega h^3}{2(1 + \beta) \nu_0}. \quad (15)$$

The applicability of this expression is demonstrated in the middle and right panels of Figure 3, where the azimuthal profiles from simulations with different viscosities are plotted in scaled azimuthal coordinates. In the middle panel density dependent viscosities and pressure are used ($\beta = 0.67$, $c_0 = 0.14h\Omega$, $\alpha = 2.15$) whereas in the right panel the simulations are performed with constant viscosity and zero pressure. The curves are obeying the azimuthal scaling very well in the region where the wakes are damped out, especially having in mind that the viscosities differ by a factor of up to 81. It turns out that the density dependence of the viscosity in form of the power law parameter β has only a small effect on the final profile especially if one accounts for the $(1 + \beta)$ factor in the scaling length aK in which case the profiles nearly match each other.

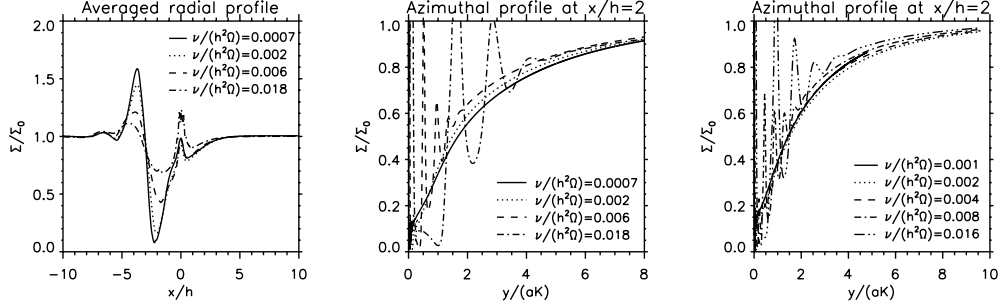


Figure 3: Comparison of gap profiles for simulations with different shear viscosities. Left and middle panel: radial and azimuthal cuts for fixed $\xi_0 = 3\nu_0$, $\beta = 0.67$, $c_0 = 0.14h\Omega$, $\alpha = 2.15$. Right panel: azimuthal cut for fixed $\xi_0 = 3\nu_0$, $\beta = 0$, $c_0 = 0h\Omega$, $\alpha = 0$.

4.3 Comparison to analytical model

The relaxation of the gap downstream from the moon can be described in terms of a linearized version of the diffusion equation (Sremčević et al., 2002)

$$\frac{\Omega_0}{2(1+\beta)\nu_0}\partial_y\Sigma = -\frac{1}{x}\partial_x^2\Sigma. \quad (16)$$

An approximate Green solution solving the problem for $\Sigma(x, y=0) = \delta(x - x_0)$ has been found (Sremčević et al., 2002) in the form

$$G(x, y, x_0) = -\frac{\sqrt{3}x_0}{2h} \left(\frac{3y}{aK}\right)^{-2/3} \exp\left[\frac{aK(x^3 + x_0^3)}{9yh^3}\right] \text{Bi}\left[\left(\frac{3y}{aK}\right)^{-2/3} \frac{x_0x}{h^2}\right] \quad (17)$$

where x and y scale with h and aK , respectively, as discussed above. $\text{Bi}(z)$ denotes the Airy function. The general solution

$$\Sigma(x, y) = \int \Sigma(x_0, y=0) G(x, y, x_0) dx_0 \quad (18)$$

can then be computed from the radial profile $\Sigma(x_0, y=0)$ after the gravitational scattering by the moon.

Figure 4 shows the the azimuthal solution alongside the azimuthal profile from the hydrodynamic simulation, where the initial radial profile $\Sigma(x_0, y=0)$, needed to calculate the analytical solution, is taken from the hydrodynamic simulation. The analytical model does not match the simulated profile

perfectly. One reason could be that Sremčević et al. (2002) have assumed a fixed boundary at $x = 0$, but in our simulations the density pattern exceeds this border.

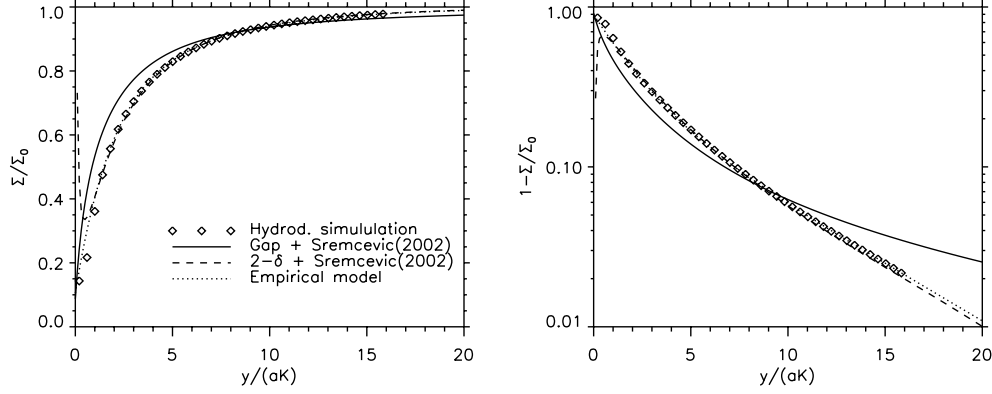


Figure 4: Comparison of the evolution of the gap minimum along the azimuth with the analytical model of Sremčević et al. (2002) and an empirical model.

It has also been shown by Sremčević et al. (2002) that the source function of the density depletion can be approximated by a combination of two or three weighted Dirac δ -functions, because the information of the exact initial profile gets quickly lost downstream from the moon. Thus, we fit additionally the approximation

$$\frac{\Sigma(x=2, y)}{\Sigma_0} = 1 - 2.35 \cdot G(x, y, -1.29) + 0.77 \cdot G(x, y, -4.4). \quad (19)$$

to the azimuthal profile where we fix the positions of the δ -functions to the mean position of the gap and the adjacent density enhancement of the general source function, but adjust the weights to fit the simulation result. This results in a very good agreement between analytical model and simulated profile for $y > 1aK$. Furthermore, we find that the empirical expression with two exponential functions

$$\frac{\Sigma(x, y)}{\Sigma_0} = 1 - 0.3 \cdot \exp\left(-0.17 \frac{y}{aK}\right) - 0.6 \cdot \exp\left(-0.55 \frac{y}{aK}\right) \quad (20)$$

also fits well the azimuthal profile in the plotted range.

4.4 The propeller Blériot and a comparison to UVIS occultation profiles

Since 2004 the spacecraft Cassini is in orbit around Saturn. Among other investigations, the Ultraviolet Imaging Spectrometer (UVIS) has recorded a number of stellar occultation observations measuring the transparency of the rings. Two occultations, ζ Persei Rev 42 in April 2007 and α Lyrae (Vega) Rev 175 in November 2012, have been fortunate to scan across the propeller structure Blériot located at a ring radius of 134,912 km. And indeed, the observations do show signatures consistent with a single density depletion and multiple enhancements at the expected location for Blériot’s gap and wake structures. This encourages us to apply our model to Blériot and compare the result with the measured optical depth. We derive UVIS optical depth profiles at a radial resolution of 200 m. These then translate into ring surface density where we assume the simplest relation $\tau/\tau_0 = \Sigma/\Sigma_0$.

The upper panel of Figure 5 shows an example of a simulation result in the region of interest where the trajectories of the occultation scans are marked by the dashed lines. Due to the excess motion of the moon (Tiscareno et al., 2010) the exact radial and azimuthal position of the moonlet is uncertain and has been adjusted so that profiles from simulation and observation fit. In the middle and lower panel the observed optical depth profiles along the occultation paths are presented together with the simulation result.

Due to the uncertainty of the ring parameters we perform a set of simulations and fit the results by eye to the data. While doing this we adjust Hill radius as well as radial and azimuthal position of the moonlet in a way that gap minimum and wake maxima are at the same location for simulations and data. In order to evaluate our fit we calculate the variance of the difference between data and model

$$\text{Var} = \frac{1}{N} \sum_{i=1}^N (\tau_{\text{d},i} - \tau_{\text{m},i})^2 \quad (21)$$

and compare it to the variance of the data points in an unperturbed region.

First, we vary the shear viscosity and fix the other simulation parameters to values expected in the Blériot region with $\beta = 2$ according to Daisaka et al. (2001), $\alpha = 1$ assuming $p = \Sigma c_0^2$ and $c_0 = 0.05 h\Omega$. Furthermore, we used $\xi_0 = 7\nu_0$ which is large enough to guarantee that no overstability occurs and a propeller pattern can form (see e.g. Schmit and Tscharnuter, 1995;

Spahn et al., 2000; Schmidt et al., 2001). The best fit of the gap region is plotted in Figure 6 (first row) and is achieved using $\nu_0 = 350 \pm 120 \text{ cm}^2/\text{s}$.

While the form of the gap is mainly maintained by the shear viscosity the form of the wake crests depends also on the action of pressure and bulk viscosity. Thus, we varied the dispersion velocity and an optimum to fit gap and wake region is found for $c_0 = (1.1 \pm 0.7) \text{ cm/s}$ (Figure 6, second and third row). The increase of the bulk viscosity to $\xi_0/\nu_0 = 10$ also improves the fit (Figure 6, forth and fifth row), but the second wake crest in the ζ Persei scan is fitted worse than when using an higher dispersion velocity. A reasonable range for the bulk viscosity is given by $7 < \xi_0/\nu_0 < 17$.

For the ζ Persei scan we find a very good agreement between observation and simulation. In the α Lyrae scan the gap is matched well, but only one of three predicted wake crests is visible. However, the three wake crests have radial width of about 100 m only, and therefore, might be obscured by the presence of self-gravity wakes, which have wave lengths in this size range (Salo, 1995). Furthermore, the neglect of the finite size of the ring particles in the hydrodynamic simulations may lead to an overestimate of the wake maxima (compare to Section 4.1).

Measurements of the ring shear viscosity are sparse in the region of the A ring between the Encke and Keeler gaps where Blériot orbits Saturn. An upper limit of $\nu = 794 \text{ cm}^2/\text{s}$ is given by Esposito et al. (1983), resulting from the analysis of the wave damping of the strong Janus 6:5 density wave by neglecting nonlinear effects. We use the parametrisation of the ring viscosity by Daisaka et al. (2001) to estimate the value of the viscosity ν of the unperturbed ring at the radial location of Blériot. This parametrisation, in the form¹

$$\nu \simeq 26 \left(\frac{r}{122\,000 \text{ km}} \right)^5 \frac{G^2 \Sigma^2}{\Omega_0^3}, \quad (22)$$

was compared by Tiscareno et al. (2007) to values of the viscosity derived from the damping of weak density waves in the inner and mid A ring, showing fairly good agreement. By using a surface mass density of 400 kg/m^2 (Colwell et al., 2009) and the semi-major axis of Blériot, we find a value of $\nu_0 = 160 \text{ cm}^2/\text{s}$ for the viscosity of the unperturbed ring. This extrapolated value is by a factor of two smaller than the viscosity value of $\nu_0 = 350 \pm 120 \text{ cm}^2/\text{s}$ estimated above.

Measurements of the dispersion velocity in the rings are rare as well, but

¹Assuming a ring particle mass density of $\rho_p = 900 \text{ kg/m}^3$.

Sremčević et al. (2008) analyzed the dispersion relation of strong density waves in the A ring and derived $c_0 = 0.3 - 0.5$ cm/s. The value for ν_0 and c_0 are much larger than the values used in our test in Section 4.1 and account for the effect of self-gravity enhancing this values. Our optimal value for the dispersion velocity $c_0 = 1.1$ cm/s is twice as larger but due to the large uncertainty still in the same range.

From Blériot’s Hill radius $h = (600 \pm 100)$ m we calculate its mass to be $M_m = (1.5 \pm 0.7) \cdot 10^{11}$ kg. It has been observed in N-body simulations that the propeller moons accrete material until they fill their Hill sphere (Lewis and Stewart, 2009). This would set the density of the moon to 490 kg/m³ and its mean radius to $R_m = 0.76 h = 460$ m (see also Porco et al., 2007).

5 Conclusions

The main results of this work are:

1. The performed hydrodynamic simulations of propeller structures in Saturn’s A-ring agree very well with results from N-body simulations.
2. The hydrodynamic simulations confirm the scaling laws for the radial and azimuthal size of a propeller, as predicted by Spahn and Sremčević (2000) and Sremčević et al. (2002).
3. The azimuthal evolution of the mass density downstream of the moonlet inferred from the hydrodynamic simulations match well the analytic solution by Sremčević et al. (2002).
4. Matching simulated optical depth profiles of the propeller Blériot to Cassini UVIS stellar occultation scans yields a Hill radius of about 600 ± 100 m, corresponding to a moonlet mass and diameter of $(1.5 \pm 0.7) \cdot 10^{11}$ kg and 900 m, respectively.
5. The comparison of optical depth profiles for the propeller Blériot and the simulations implies a shear viscosity of the ring of $\nu = (350 \pm 120)$ cm²/s, a bulk viscosity in the range $7 < \xi_0/\nu_0 < 17$ and a dispersion velocity of $c_0 = (1.1 \pm 0.7)$ cm/s.

The isothermal model works surprisingly well to describe the density pattern of the propeller, especially for the gap profiles. However, non-isothermal

effects might influence the viscosity of the ring material, and thus, the propeller structure. Furthermore, a locally enhanced dispersion velocity would also cause an enhanced local thickness of the ring, as it has been observed for the propeller Earhart around Saturn’s vernal equinox (Hoffmann et al., 2013, 2015). However, the stars ζ Persei and α Lyrae were observed with a rather high elevation angle of 35 and 38 degrees, respectively, during the occultations and the vertical structure should be here of minor importance. Moreover, the inclusion of ring self-gravity in the model would allow to investigate the influence of the self-gravity wakes on the propeller, especially in the moonlet wake region, but this is left for future work.

Acknowledgement

This work has been supported by the Deutsches Zentrum für Luft-und Raumfahrt (OH 1401) and the Deutsche Forschungsgemeinschaft (Sp 384/28-1, Ho5720/1-1).

References

- Borderies, N., Goldreich, P., Tremaine, S., Aug. 1989. The formation of sharp edges in planetary rings by nearby satellites. *Icarus* 80, 344–360.
- Colwell, J. E., Nicholson, P. D., Tiscareno, M. S., Murray, C. D., French, R. G., Marouf, E. A., 2009. The Structure of Saturn’s Rings. In: Dougherty, M. K., Esposito, L. W., Krimigis, S. M. (Eds.), *Saturn from Cassini-Huygens*. Springer Verlag, Ch. 13, pp. 375–412.
- Cuzzi, J. N., Scargle, J. D., May 1985. Wavy edges suggest moonlet in Encke’s gap. *Astrophysical Journal* 292, 276–290.
- Daisaka, H., Tanaka, H., Ida, S., Dec. 2001. Viscosity in a Dense Planetary Ring with Self-Gravitating Particles. *Icarus* 154, 296–312.
- Dermott, S. F., Murray, C. D., Oct. 1981. The dynamics of tadpole and horseshoe orbits. I - Theory. II - The coorbital satellites of Saturn. *Icarus* 48, 1–22.
- Dermott, S. F., Murray, C. D., Sinclair, A. T., Mar. 1980. The narrow rings of Jupiter, Saturn and Uranus. *Nature* 284, 309–313.

- Esposito, L. W., Ocallaghan, M., West, R. A., 1983. The structure of Saturn's rings - Implications from the Voyager stellar occultation. *Icarus* 56, 439–452.
- Henon, M., Sep. 1981. A simple model of Saturn's rings. *Nature* 293, 33–35.
- Hertzsch, J.-M., Scholl, H., Spahn, F., Katzorke, I., Apr. 1997. Simulation of collisions in planetary rings. *Astronomy and Astrophysics* 320, 319–324.
- Hill, G., 1878. Researches in the lunar theory. *Am. J. Math.* 1, 5–26.
- Hoffmann, H., Seiß, M., Salo, H., Spahn, F., May 2015. Vertical structures induced by embedded moonlets in Saturn's rings. *Icarus* 252, 400–414.
- Hoffmann, H., Seiß, M., Spahn, F., Mar. 2013. Vertical Relaxation of a Moonlet Propeller in Saturn's A Ring. *Astrophysical Journal Letters* 765, L4.
- Kley, W., Mar. 1999. Mass flow and accretion through gaps in accretion discs. *Monthly Notices Royal Astron. Soc.* 303, 696–710.
- LeVeque, R. J., 2002. *Finite Volume Methods for Hyperbolic Problems*. Cambridge University Press.
- Lewis, M. C., Stewart, G. R., Dec. 2000. Collisional Dynamics of Perturbed Planetary Rings. I. *Astronomical Journal* 120, 3295–3310.
- Lewis, M. C., Stewart, G. R., Nov. 2005. Expectations for Cassini observations of ring material with nearby moons. *Icarus* 178, 124–143.
- Lewis, M. C., Stewart, G. R., Feb. 2009. Features around embedded moonlets in Saturn's rings: The role of self-gravity and particle size distributions. *Icarus* 199, 387–412.
- Lissauer, J. J., Shu, F. H., Cuzzi, J. N., Aug. 1981. Moonlets in Saturn's rings. *Nature* 292, 707–711.
- Lubow, S. H., Seibert, M., Artymowicz, P., Dec. 1999. Disk Accretion onto High-Mass Planets. *Astrophysical Journal* 526, 1001–1012.
- Petit, J.-M., Henon, M., Jun. 1988. A numerical simulation of planetary rings. III - Mass segregation, ring confinement, and gap formation. *Astronomy and Astrophysics* 199, 343–356.

- Porco, C. C., May 2005. S/2005 S 1. IAU Circ. 8524, 1.
- Porco, C. C., Thomas, P. C., Weiss, J. W., Richardson, D. C., Dec. 2007. Saturn's Small Inner Satellites: Clues to Their Origins. *Science* 318, 1602–.
- Rein, H., Papaloizou, J. C. B., 2010. Stochastic orbital migration of small bodies in Saturn's rings. *Astronomy and Astrophysics* 524, A22.
- Salo, H., Oct. 1995. Simulations of dense planetary rings. III. Self-gravitating identical particles. *Icarus* 117, 287–312.
- Salo, H., Schmidt, J., Spahn, F., Oct. 2001. Viscous Overstability in Saturn's B Ring. I. Direct Simulations and Measurement of Transport Coefficients. *Icarus* 153, 295–315.
- Schmidt, J., Salo, H., Spahn, F., Petzschmann, O., Oct. 2001. Viscous Overstability in Saturn's B-Ring. II. Hydrodynamic Theory and Comparison to Simulations. *Icarus* 153, 316–331.
- Schmit, U., Tscharnuter, W. M., Jun. 1995. A fluid dynamical treatment of the common action of self-gravitation, collisions, and rotation in Saturn's B-ring. *Icarus* 115, 304–319.
- Seiß, M., Spahn, F., 2011. Hydrodynamics of saturns dense rings. *Mathematical Modelling of Natural Phenomena* 6 (04), 191–218.
URL <http://dx.doi.org/10.1051/mmnp/20116409>
- Seiß, M., Spahn, F., Schmidt, J., Nov. 2010. Moonlet induced wakes in planetary rings: Analytical model including eccentric orbits of moon and ring particles. *Icarus* 210, 298–317.
- Seiß, M., Spahn, F., Sremčević, M., Salo, H., Jun. 2005. Structures induced by small moonlets in Saturn's rings: Implications for the Cassini Mission. *Geophysical Research Letters* 32, 11205.
- Showalter, M. R., Jun. 1991. Visual detection of 1981S13, Saturn's eighteenth satellite, and its role in the Encke gap. *Nature* 351, 709–713.
- Showalter, M. R., Cuzzi, J. N., Marouf, E. A., Esposito, L. W., May 1986. Satellite 'wakes' and the orbit of the Encke Gap moonlet. *Icarus* 66, 297–323.

- Spahn, F., Schmidt, J., Petzschmann, O., Salo, H., Jun. 2000. Note: Stability analysis of a Keplerian disk of granular grains: Influence of thermal diffusion. *Icarus* 145, 657–660.
- Spahn, F., Scholl, H., Hertzsch, J., Oct. 1994. Structures in planetary rings caused by embedded moonlets. *Icarus* 111, 514–535.
- Spahn, F., Sponholz, H., Jun. 1989. Existence of moonlets in Saturn’s rings inferred from the optical depth profile. *Nature* 339, 607–608.
- Spahn, F., Sremčević, M., Jun. 2000. Density patterns induced by small moonlets in Saturn’s rings? *Astronomy and Astrophysics* 358, 368–372.
- Spahn, F., Wiebicke, H.-J., Jan. 1989. Long-term gravitational influence of moonlets in planetary rings. *Icarus* 77, 124–134.
- Sremčević, M., Schmidt, J., Salo, H., Seiß, M., Spahn, F., Albers, N., Oct. 2007. A belt of moonlets in Saturn’s A ring. *Nature* 449, 1019–1021.
- Sremčević, M., Stewart, G. R., Albers, N., Colwell, J. E., Esposito, L. W., Sep. 2008. Density Waves in Saturn’s Rings: Non-linear Dispersion and Moon Libration Effects. In: *Bulletin of the American Astronomical Society*. Vol. 40 of *Bulletin of the American Astronomical Society*.
- Sremčević, M., Spahn, F., Duschl, W. J., Dec. 2002. Density structures in perturbed thin cold discs. *Monthly Notices Royal Astron. Soc.* 337, 1139–1152.
- Tiscareno, M. S., Burns, J. A., Hedman, M. M., Porco, C. C., Mar. 2008. The Population of Propellers in Saturn’s A Ring. *Astronomical Journal* 135, 1083–1091.
- Tiscareno, M. S., Burns, J. A., Hedman, M. M., Porco, C. C., Weiss, J. W., Dones, L., Richardson, D. C., Murray, C. D., Mar. 2006. 100-metre-diameter moonlets in Saturn’s A ring from observations of ‘propeller’ structures. *Nature* 440, 648–650.
- Tiscareno, M. S., Burns, J. A., Nicholson, P. D., Hedman, M. M., Porco, C. C., Jul. 2007. Cassini imaging of Saturn’s rings. II. A wavelet technique for analysis of density waves and other radial structure in the rings. *Icarus* 189, 14–34.

Tiscareno, M. S., Burns, J. A., Sremčević, M., Beurle, K., Hedman, M. M., Cooper, N. J., Milano, A. J., Evans, M. W., Porco, C. C., Spitale, J. N., Weiss, J. W., Aug. 2010. Physical Characteristics and Non-Keplerian Orbital Motion of "Propeller" Moons Embedded in Saturn's Rings. *Astrophysical Journal Letters* 718, L92–L96.

Weiss, J. W., Porco, C. C., Tiscareno, M. S., Jul. 2009. Ring Edge Waves and the Masses of Nearby Satellites. *Astronomical Journal* 138, 272–286.

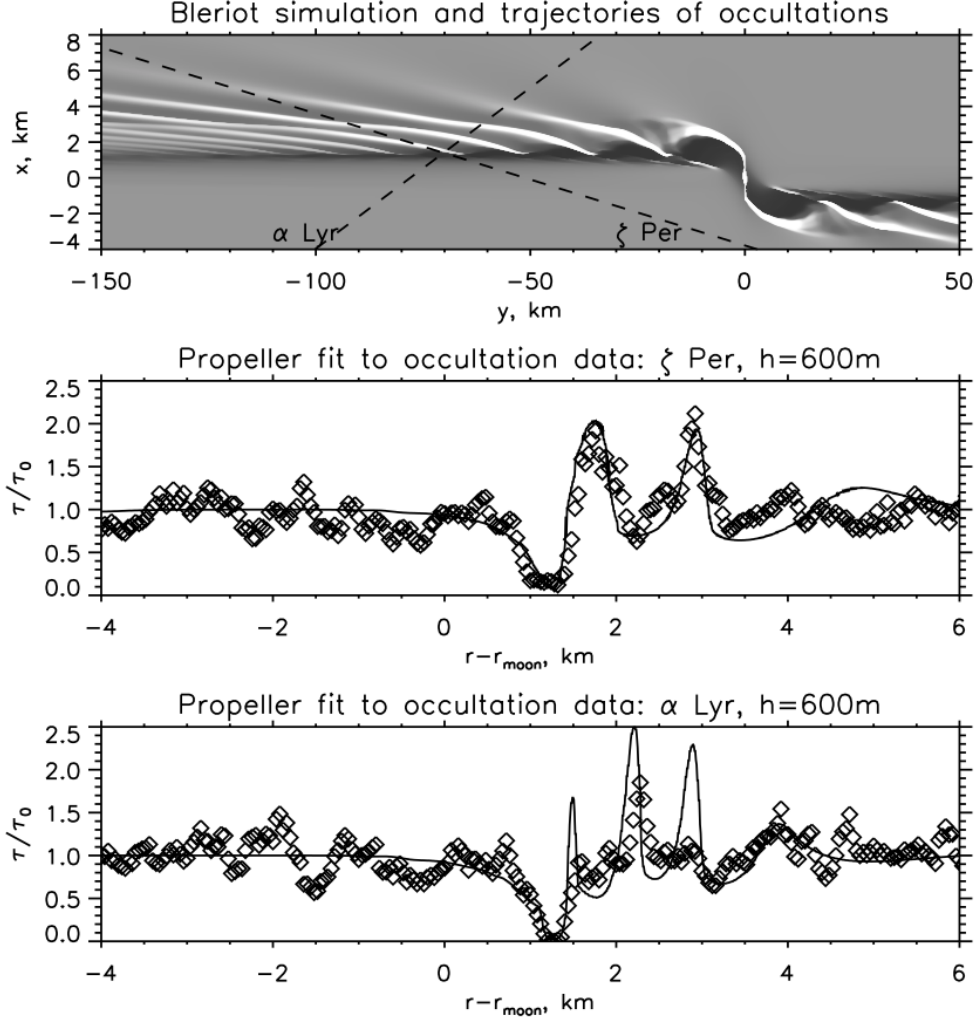


Figure 5: Comparison of a Blériot propeller simulation with two optical depth profiles. Upper panel: density of simulation and trajectories of the UVIS occultation scans. Middle and lower panel: the symbols represent the optical depth from UVIS occultations of the stars ζ Persei and α Lyrae, respectively, where the line denotes the simulation results using $c_0 = 0.05 h\Omega$, $\alpha = 1$, $\nu_0 = 0.00075 h^2\Omega$, $\xi_0 = 0.035 h^2\Omega$ and $\beta = 2$.

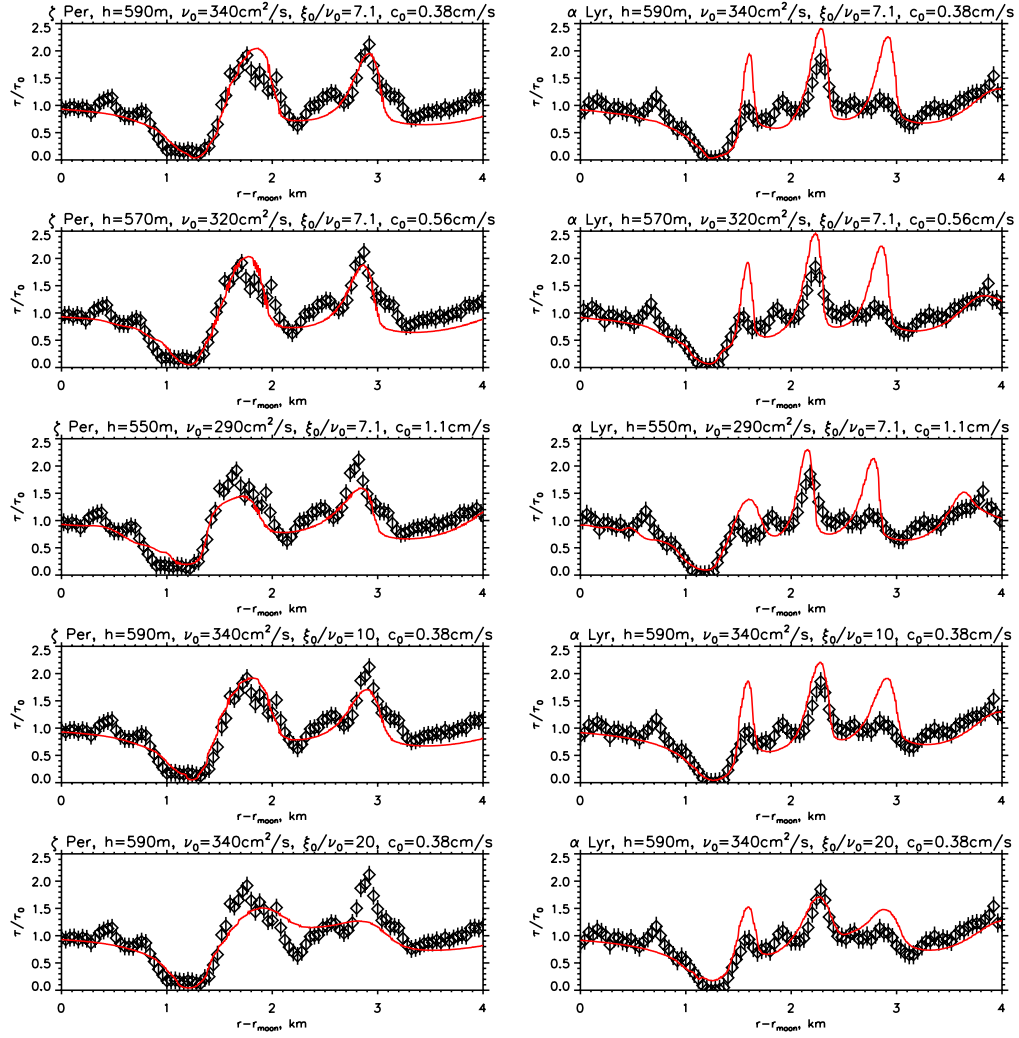


Figure 6: Comparison of a Blériot propeller simulation with two optical depth profiles for different simulation parameter.